Proceedings of IMECE'02
2002 ASME International Mechanical Engineering Congress and Exposition
November 17-22, 2002, New Orleans, Louisiana, USA

IMECE/2002-32943

MODELING APPROACHES TO HYPERSONIC AEROELASTICITY

B.J. Thuruthimattam, P.P. Friedmann*, J.J. McNamara and K.G. Powell
Department of Aerospace Engineering
University of Michigan
Ann Arbor, Michigan 48109-2140
Email: peretzf@umich.edu

ABSTRACT

The hypersonic aeroelastic problem of a double wedge airfoil typical cross-section is studied using three different unsteady aerodynamic loads: (1) third order piston theory, (2) Euler solution, and (3) unsteady Navier-Stokes aerodynamics. Computational aeroelastic response results are obtained, and compared with piston theory solutions for a variety of flight conditions. Aeroelastic behavior is studied for $7 < M < 15$ at an altitude of 70,000 feet. A parametric study of offsets and wedge angles is conducted. Piston theory and Euler solutions are fairly close below the flutter boundary, and differences increase with increase in Mach number, close to the flutter boundary. Differences between viscous and inviscid aeroelastic behavior can be substantial. The results presented serve as a partial validation of the CFL3D code for the hypersonic flight regime.

NOMENCLATURE

a Nondimensional offset between the elastic axis and the mid-chord
a_∞ Speed of sound
b Semi-chord
c Reference length, chord length of double wedge airfoil
C_L, C_D, C_{My} Coefficients of lift, drag and moment about the y-axis
$C_{p,PT}, C_{p,NS}$ Piston theory pressure coefficient, and CFD Navier-Stokes pressure coefficient respectively
$f(x)$ Function describing airfoil surface
h Airfoil vertical displacement at elastic axis
I_α Mass moment of inertia about the elastic axis
K_α, K_h Spring constants in pitch and plunge respectively; $K_\alpha = I_\alpha \omega_\alpha^2, K_h = m\omega_h^2$
L Lift per unit span
M Free stream Mach number
$\mathbf{M}, \mathbf{K}$ Generalized mass and stiffness matrices of the structure
m Mass per unit span
M_{EA} Moment per unit span about the elastic axis
n_m Number of modes used
p Pressure
$\mathbf{Q}$ Generalized force vector for the structure
Q_i Generalized force corresponding to mode i
q_∞ Dynamic pressure
q_i Modal amplitude of mode i
r_α Nondimensional radius of gyration
S Surface area of the structure
S_α Static mass moment of wing section about elastic axis
T Kinetic energy of the structure
t Time
t_h Airfoil half thickness
U Potential energy of the structure
V Free stream velocity
v_n Normal velocity of airfoil surface
x_α Nondimensional offset between the elastic axis and the cross-sectional center of gravity
x, y, z Spatial Coordinates
$Z(x,y,t)$ Position of structural surface
α Airfoil pitch displacement about the elastic axis
γ Ratio of specific heats
μ_m Mass ratio

*Address all correspondence to this author.

ρ Air density

ω_α, ω_h Natural frequencies of uncoupled pitch and plunge motions

ω_1, ω_2 Natural frequencies of double wedged airfoil

ϕ_i Mode shape for mode i

τ Thickness ratio; $\tau = \frac{t_h}{b}$

$\dot{()}, \ddot{()}$ First and second derivatives with respect to time

$()_u, ()_l$ Of the upper and lower surface, respectively

INTRODUCTION AND PROBLEM STATEMENT

In recent years, renewed activity in hypersonic flight research has been stimulated by the current need for a low cost, single-stage-to-orbit (SSTO) or two-stage-to-orbit (TSTO) reusable launch vehicle (RLV) and the long term design goal of incorporating air breathing propulsion devices in this class of vehicles. The X-33, an example of the former vehicle type, was a 1/2 scale, fully functional technology demonstrator for the full scale VentureStar. Another ongoing hypersonic vehicle research program is the NASA Hyper-X experimental vehicle effort. Other activities are focused on the design of unmanned hypersonic vehicles that meet the needs of the US Air Force. The present study is aimed at enhancing the fundamental understanding of the aeroelastic behavior of vehicles that belong to this category and operate in a typical hypersonic flight envelope.

Vehicles in this category are based on a lifting body design. However, stringent minimum-weight requirements imply a degree of fuselage flexibility. Aerodynamic surfaces, needed for control, are also flexible. Furthermore, to meet the requirement of a flight profile that spans the Mach number range from 0 to 15, the vehicle must withstand severe aerodynamic heating. These factors combine to produce unusual aeroelastic problems that have received only limited attention in the past. Furthermore, it is important to emphasize that testing of aeroelastically scaled wind tunnel models, a conventional practice in subsonic and supersonic flow, is not feasible in the hypersonic regime. Thus, the role of aeroelastic simulations is more important for this flight regime than in any other flight regime.

Previous studies in this area can be separated into several groups. The first group consists of studies focusing on panel flutter, which is a localized aeroelastic problem representing a small portion of the skin on the surface of the hypersonic vehicle. Hypersonic panel flutter has been studied by a number of researchers, focusing on important effects such as aerodynamic heating [1], composite [2, 3] and nonlinear structural models [4], and initial panel curvature [5]. A comprehensive review of this research can be found in a recent survey paper [6]. A fundamental question associated with these studies, is whether piston theory, which has been widely used in the Mach number range, $1.8 < M < 5.0$ is an appropriate tool for modeling unsteady aerodynamic loads on the surface of a hypersonic vehicle. This was considered in Ref. [5], where the unsteady pressure coefficient on the surface of a typical panel, undergoing prescribed oscillations at frequencies representative of a typical panel in hypersonic flow, was computed using: third-order piston theory, an exact solution of the nonlinear Euler equations, and a numerical solution of the unsteady Navier-Stokes equations. At a typical hypersonic Mach number (M=10), results from the third-order piston theory are within 5% of the exact solution of the Euler equations. However, a difference of approximately 60% exists between the Euler solution and the solution based on the Navier-Stokes equations. This implies that the accurate representation of the unsteady aerodynamic loading, at certain flight conditions, will require the solution of the Navier-Stokes equations. Another implication of this statement is that the heat transfer problem may have to be coupled with the aeroelastic analysis of a hypersonic vehicle for certain portions of the flight envelope.

The second group of studies in this area was motivated by a previous hypersonic vehicle, namely the National Aerospace Plane (NASP). Representative studies in this category are Refs. [7-11]. However, some of these studies dealt with the transonic regime, because it was perceived to be a critical region and the NASA Langley facilities (the Transonic Dynamics Wind Tunnel) were appropriate for testing vehicle behavior in this Mach number range. In Ref. [9], Spain et al. carried out a flutter analysis of all-moveable NASP-like wings with slab and double wedge airfoils. They found that using effective shapes for the airfoils obtained by adding the boundary layer displacement thickness to the airfoil thickness improved the overall agreement with experiments.

The third group of studies is restricted to recent papers that deal with the newer hypersonic configurations such as the X-33 or the X-34. Reference [12] considered the X-34 launch vehicle in free flight at M=8.0, and then reinterpreted these results at different flight conditions using dynamic pressure and altitude corrections. The aeroelastic instability of a generic hypersonic vehicle, resembling the X-33, was considered in Ref. [13]. It was found that at high hypersonic speeds and high altitudes, the hypersonic vehicle is stable, when piston theory is used to represent the aerodynamic loads. Sensitivity of the flutter boundaries to vehicle flexibility and trim state were also considered [13]. In another reference [14], CFD-based flutter analysis was used for the aeroelastic analysis of the X-43 configuration, using system identification based order reduction of the aerodynamic degrees of freedom. Both the structure and the fluid were discretized using the finite element approach. It was shown that piston theory and ARMA Euler calculations predicted somewhat similar results.

From the studies on various hypersonic vehicles (Refs. [7, 14–16]), one can identify operating envelopes for each vehicle. One can obtain a convenient graphical representation of operating conditions for this class of vehicles, shown in Fig. 1, by combining these envelopes.

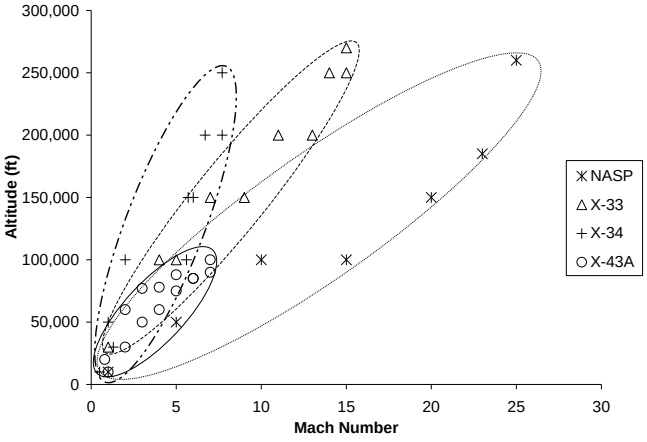

Figure 1. OPERATING ENVELOPES FOR SEVERAL MODERN HYPERSONIC VEHICLES.

In a recent study [17], the authors of this paper developed an aeroelastic analysis capability for generic hypersonic vehicles in the Mach number range $0.5 < M < 15$, using computational aeroelasticity. The computational tool consisted of the CFL3D code, developed by NASA Langley, combined with a finite element model of a generic hypersonic vehicle utilizing NASTRAN. During the validation process of the analysis [17], the authors studied the aeroelastic behavior of a two dimensional double wedge airfoil, operating in the Mach number range of $2.0 < M < 15.0$. It was found that the double wedge airfoil is an excellent vehicle for studying aeroelastic behavior in hypersonic flow. Therefore, the current paper is aimed at studying several important aspects of computational hypersonic aeroelasticity based on the double wedge airfoil. The specific objectives of this paper are:

1. Develop an aeroelastic analysis for a double wedge airfoil in hypersonic flow using third-order piston theory.
2. Determine the time-step requirements for the reliable computation of the unsteady airloads for this particular problem when using the Euler and Navier-Stokes options of CFL3D.
3. Compare the aeroelastic behavior predicted by the simple piston theory analysis with refined solutions for the same problem, using CFL3D, with both Euler and Navier-Stokes solutions for the unsteady aerodynamic loads.
4. Compare the exact solutions for aeroelastic behavior using the Navier-Stokes-based unsteady airloads, with approximate solutions based on an airfoil shape modified by the presence of a boundary layer.
5. Conduct a parametric study that illustrates the effect of offsets between elastic axis, aerodynamic center and wedge angle of the airfoil.

Finally, it is important to note that these objectives not only enhance our understanding of hypersonic aeroelasticity, but also make a valuable contribution towards the validation of the CFL3D code for hypersonic flight conditions.

METHOD OF SOLUTION

An overview of the solution of the computational aeroelasticity problem is shown in Fig. 2. First, the vehicle geometry is created using CAD software, and from this geometry a mesh generator is used to create a structured mesh for the flow domain around the body. In parallel, an unstructured mesh is created for the finite element model of the structure using the same nodes on the vehicle surface that were used to generate for the fluid mesh. Subsequently, the fluid mesh is used to compute the flow around the rigid body using a CFD solver, while the structural mesh is used to obtain the free vibration modes of the structure by finite element analysis. Matching surface nodes in both meshes by their coordinates, the modal displacements at each fluid node are set to those of the appropriate node on the structural mesh, and thus the mode shape data for CFL3D is generated. Using the flow solution as an initial condition, and the modal information, an aeroelastic steady state is obtained. Next, the structure is perturbed in one or more of its modes by an initial modal velocity condition, and the transient response of the structure is obtained. To determine the flutter conditions at a given altitude, aeroelastic transients are computed at several Mach numbers and the corresponding dynamic pressures. The frequency and damping characteristics of the transient response at each Mach number can be determined from a moving block approach [18], and the flutter Mach number associated with this altitude can be estimated by interpolation.

Euler/Navier-Stokes Aeroelastic Option in CFL3D

The aeroelastic analysis of the double wedge airfoil is carried out using the CFL3D code [19]. The code uses an implicit, finite-volume algorithm based on upwind-biased spatial differencing to solve the time-dependent Euler and Reynolds-averaged Navier-Stokes equations. Multigrid and mesh-sequencing are available for convergence acceleration. The algorithm, which is based on a cell-centered scheme, uses upwind-differencing based on either flux-vector splitting or flux-difference splitting, and can sharply capture shock waves. For applications utilizing the thin-layer Navier-Stokes equations, different turbulence models are available. For time-accurate problems using a deforming mesh, an additional term accounting for the change in cell-volume is included in the time-discretization of the governing equations. Since CFL3D is an implicit code using approximate factorization, linearization and factorization errors are introduced at every time-step. Hence, intermediate calculations referred to as "subiterations" are used to reduce these errors. Increasing these subiterations improves the accuracy of the simulation, albeit at

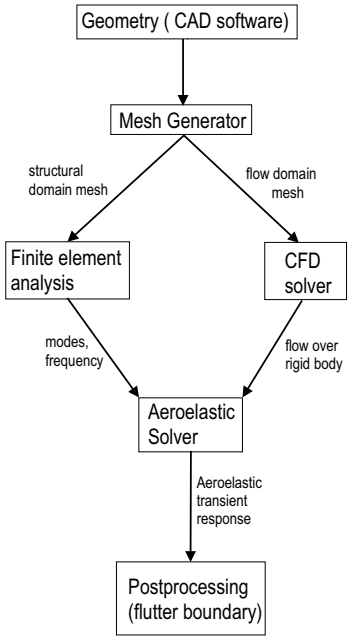

Figure 2. A FLOW DIAGRAM OF THE COMPUTATIONAL AEROELASTIC SOLUTION PROCEDURE.

increased computational cost.

The aeroelastic approach underlying the CFL3D code is similar to that described in Refs. [20, 21]. In this formulation, the equations are derived by assuming that the general motion $w(x,y,t)$ of the structure is described by a separation of time and space variables in a finite modal series. The free vibration modes in this study were obtained from a finite element model of the vehicle. The displacements on the vehicle are obtained from a modal series, given next.

$$Z(x,y,t) = \sum_{i=1}^{n_m} q_i(t)\phi_i(x,y) \tag{1}$$

The equations of motion are based on Lagrange's equations,

$$\frac{d}{dt}\left(\frac{\partial T}{\partial \dot{q}_i}\right) - \frac{\partial T}{\partial q_i} + \frac{\partial U}{\partial q_i} = Q_i, \qquad i = 1,2,... \tag{2}$$

The resulting set of equations of motion is

$$\mathbf{M}\ddot{q} + \mathbf{K}q = \mathbf{Q}(\mathbf{q},\dot{\mathbf{q}},\ddot{\mathbf{q}}), \qquad \mathbf{q}^T = [q_1\, q_2 ...] \tag{3}$$

where the elements of the generalized force vector are given by,

$$Q_i = \frac{\rho V^2}{2} c^2 \int_S \phi_i \frac{\Delta p \; dS}{\rho V^2/2 \; c^2} \tag{4}$$

From Eq. (3),

$$\ddot{\mathbf{q}} = -\mathbf{M}^{-1}\mathbf{K}\mathbf{q} + \mathbf{M}^{-1}\mathbf{Q} \tag{5}$$

The aeroelastic equations are written in terms of a linear state-space equation (using a state vector of the form $[... \; \dot{q}_{i-1} \; q_i \; \dot{q}_i \; q_{i+1} \; ...]^T$) such that a modified state-transition-matrix integrator can be used to march the coupled fluid-structural system forward in time. The fluid forces are coupled with the structural equations of motion through the generalized aerodynamic forces. Thus, a time-history of the modal displacements, modal velocities and generalized forces is obtained.

The aeroelastic capabilities of CFL3D, based on this modal response approach for obtaining the flutter boundary, have been partially validated for the transonic regime for the first AGARD standard aeroelastic configuration for dynamic response, Wing 445.6. The results of flutter calculations using Euler aerodynamics are given in Ref. [22] and those using Navier-Stokes aerodynamics are given in Ref. [23].

Computational Model of the Double Wedge Airfoil

Validation of the CFL3D code for the hypersonic regime has never been undertaken. Therefore, reliable results for a fairly simple configuration for which aeroelastic stability and response results could be generated independently, were essential. A typical cross-section based on the double wedge airfoil, shown in Figs. 3 and 4, met these requirements. Generating results for this configuration using Euler and Navier-Stokes unsteady aerodynamic loads, and comparing them with results obtained using an independently developed aeroelastic code based on third-order piston theory, provides a reliable means for validating CFL3D in the hypersonic regime.

The Euler and Navier-Stokes computations are carried out using a 225×65 C-grid with 225 points around the wing and its wake (145 points wrapped around the airfoil itself), and 65 points extending radially outward from the airfoil surface. The computational domain extends one chord-length upstream and six chord lengths downstream, and one chord length to the upper and lower boundaries. For the Navier-Stokes simulations, the Spalart-Allmaras turbulence model was used, along with an adiabatic wall temperature condition. The double wedge airfoil and a portion of the surrounding computational grid are shown in Fig. 3.

Aeroelastic Model for a Double Wedge Airfoil Using Higher Order Piston Theory

Piston theory is an inviscid unsteady aerodynamic theory, used extensively in supersonic and hypersonic aeroelasticity, which provides a point-function relationship between the local pressure on the surface of the vehicle and the component of fluid

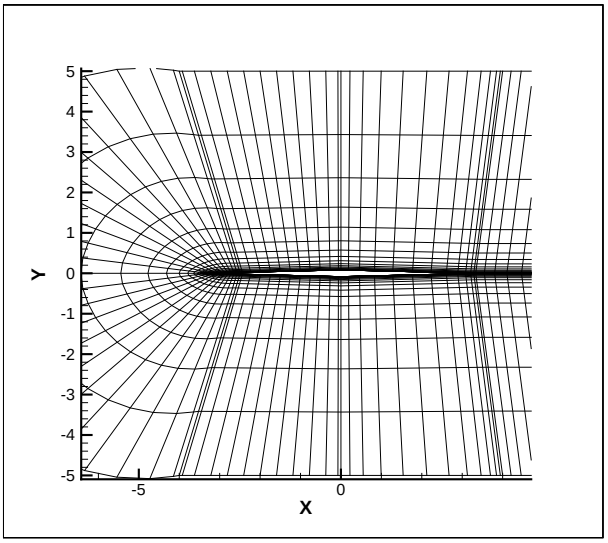

Figure 3. DOUBLE WEDGE AIRFOIL SECTION, AND SURROUNDNIG GRID, TO SCALE.

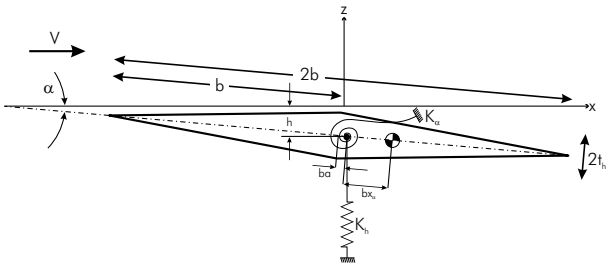

Figure 4. TWO DEGREE-OF-FREEDOM TYPICAL AIRFOIL GEOMETRY.

velocity normal to the moving surface [24, 25]. The derivation utilizes the isentropic "simple wave" expression for the pressure on the surface of a moving piston,

$$\frac{p(x,t)}{p_\infty} = \left(1 + \frac{\gamma-1}{2}\frac{v_n}{a_\infty}\right)^{\frac{2\gamma}{(\gamma-1)}} \tag{6}$$

where

$$v_n = \frac{\partial Z(x,t)}{\partial t} + V\frac{\partial Z(x,t)}{\partial x} \tag{7}$$

The expression for piston theory is based on a binomial expansion of Eq. (6), where the order of the expansion is determined by the ratio of $\frac{v_n}{a_\infty}$. Reference [25] suggested a third-order expansion, since it produced the smallest error of the various orders of expansion used when compared to the limiting values of pressure, namely the "simple wave" and "shock expansion" solutions. The third-order expansion of Eq. (6) yields

$$p(x,t) - p_\infty = p_\infty\left[\gamma\frac{v_n}{a_\infty} + \frac{\gamma(\gamma+1)}{4}\left(\frac{v_n}{a_\infty}\right)^2 + \frac{\gamma(\gamma+1)}{12}\left(\frac{v_n}{a_\infty}\right)^3\right] \tag{8}$$

An aeroelastic analysis for a typical cross-section for a double wedge airfoil was developed using Eq. (8) for the unsteady pressure loading. A typical cross-section, with the usual pitch and plunge degrees of freedom, shown in Fig. 4, was used to obtain the equations of motion from Lagrange's equations.

$$\begin{aligned} m\ddot{h} + S_\alpha\ddot{\alpha} + K_h h &= -L(t) \\ S_\alpha\ddot{h} + I_\alpha\ddot{\alpha} + K_\alpha\alpha &= M_{EA}(t) \end{aligned} \tag{9}$$

From Fig. 4, it is evident that for small displacements,

$$Z(x,t) = -\{h(t) + (x - ba)\alpha(t)\} + f(x) \tag{10}$$

and

$$\begin{aligned} v_{n,u} &= -\{\dot{h} + (x-ba)\dot{\alpha}\} + V\left\{-\alpha + \frac{\partial f(x)}{\partial x}\right\} \\ v_{n,l} &= \{\dot{h} + (x-ba)\dot{\alpha}\} - V\left\{-\alpha + \frac{\partial f(x)}{\partial x}\right\} \end{aligned} \tag{11}$$

where

$$\begin{aligned} \frac{\partial f_u(x)}{\partial x} &= \tau \;: -b < x < 0 \\ \frac{\partial f_u(x)}{\partial x} &= -\tau : \quad 0 < x < b \\ \frac{\partial f_l(x)}{\partial x} &= -\tau : -b < x < 0 \\ \frac{\partial f_l(x)}{\partial x} &= \tau \;: \quad 0 < x < b \end{aligned} \tag{12}$$

From Eqs. (8), (11), and (12) the unsteady pressure distribution was determined. The unsteady lift and moment due to this pressure distribution was determined from

$$\begin{aligned} L(t) &= \int_{-b}^{b}\left(p_l(x,t) - p_u(x,t)\right)dx \\ M_{EA}(t) &= -\int_{-b}^{b}(x-ba)\left(p_l(x,t) - p_u(x,t)\right)dx \end{aligned} \tag{13}$$

The unsteady lift is given by

$$L(t) = L_1(t) + L_2(t) + L_3(t) \tag{14}$$

where,

$$\begin{aligned}
L_1(t) &= 4P_\infty \gamma M b \left\{ \tfrac{\dot{h}}{V} - ba\tfrac{\dot{\alpha}}{V} + \alpha \right\} \\
L_2(t) &= -P_\infty \gamma(\gamma+1) M^2 b^2 \tau \left(\tfrac{\dot{\alpha}}{V}\right) \\
L_3(t) &= \tfrac{1}{3} P_\infty \gamma(\gamma+1) M^3 b \left\{ \left(\tfrac{\dot{h}}{V} - ba\tfrac{\dot{\alpha}}{V} + \alpha \right) \right. \\
&\quad \left. \left(\left(\tfrac{\dot{h}}{V} - ba\tfrac{\dot{\alpha}}{V} + \alpha \right)^2 + 3\tau^2 + \left(b\tfrac{\dot{\alpha}}{V} \right)^2 \right) \right\}
\end{aligned} \tag{15}$$

Note that $L_1(t)$, $L_2(t)$, and $L_3(t)$ represent the first, second, and third-order piston theory lift components respectively. Similarly, the unsteady moment is given by,

$$M_{EA}(t) = M_1(t) + M_2(t) + M_3(t) \tag{16}$$

where

$$\begin{aligned}
M_1(t) &= 4P_\infty \gamma M b^2 \left\{ a\tfrac{\dot{h}}{V} - \left(\tfrac{b}{3} + b\,a^2 \right) \tfrac{\dot{\alpha}}{V} + a\alpha \right\} \\
M_2(t) &= P_\infty \gamma(\gamma+1) M^2 b^2 \tau \left\{ \tfrac{\dot{h}}{V} - 2ba\tfrac{\dot{\alpha}}{V} + \alpha \right\} \\
M_3(t) &= -\tfrac{1}{3} P_\infty \gamma(\gamma+1) M^3 b^2 \left\{ \tfrac{1}{5} \left(b\tfrac{\dot{\alpha}}{V} \right)^3 \right. \\
&\quad -a \left(\tfrac{\dot{h}}{V} - ba\tfrac{\dot{\alpha}}{V} + \alpha \right) \left(\left(\tfrac{\dot{h}}{V} - ba\tfrac{\dot{\alpha}}{V} + \alpha \right)^2 + 3\tau^2 \right) \\
&\quad +b\tfrac{\dot{\alpha}}{V} \left(\left(\tfrac{\dot{h}}{V} - ba\tfrac{\dot{\alpha}}{V} + \alpha \right)^2 + \tau^2 \right. \\
&\quad \left. \left. -ba\tfrac{\dot{\alpha}}{V} \left(\tfrac{\dot{h}}{V} - ba\tfrac{\dot{\alpha}}{V} + \alpha \right) \right) \right\}
\end{aligned} \tag{17}$$

Again, $M_1(t)$, $M_2(t)$, and $M_3(t)$ represent the first, second, and third-order piston theory moment components respectively.

For comparison with CFL3D, it is convenient to represent Eq. (9) in terms generalized coordinates and forces. Therefore, a normal mode transformation is used such that:

$$\begin{Bmatrix} h(t) \\ \alpha(t) \end{Bmatrix} = [\phi_1 \, \phi_2] \begin{Bmatrix} q_1(t) \\ q_2(t) \end{Bmatrix} \tag{18}$$

Substituting Eq. (18) into Eq. (9), and premultiplying by the transpose of the modal matrix yields

$$\begin{Bmatrix} \ddot{q_1}(t) \\ \ddot{q_2}(t) \end{Bmatrix} = [\phi_1 \, \phi_2]^T \begin{Bmatrix} L(t) \\ M_{EA}(t) \end{Bmatrix} - \begin{bmatrix} \omega_1^2 & 0 \\ 0 & \omega_2^2 \end{bmatrix} \begin{Bmatrix} q_1(t) \\ q_2(t) \end{Bmatrix} \tag{19}$$

for mass normalized modes.

Note that the modal amplitudes are coupled through the generalized forces. Equation (19) was solved using the subroutine ODE45 in MATLAB©.

Calculation of Effective Shape of the Double Wedge Airfoil

As indicated in Ref. [26], the thick boundary layer in hypersonic flow can exert a major displacement effect on the outer inviscid flow, causing a given body shape to appear much thicker. This influences the surface pressure distribution, and it also effects vehicle aeroelastic stability. To incorporate this effect in an approximate manner, a static boundary layer displacement thickness is used in conjunction with piston theory. A similar approach was considered in Ref. [9], where a flat-plate boundary layer thickness was used. In order to improve the level of accuracy in the displacement thickness, the steady pressure distribution calculated from a CFD based Navier-Stokes solution is used to generate the effective airfoil shape. The steady component of the piston theory pressure can be obtained from Eq.(8) by neglecting all time dependent terms. For zero angle of attack, this is given by:

$$C_{p,PT}(x) = \frac{p_\infty}{q_\infty} \left\{ \gamma M \frac{dZ}{dx} + \frac{\gamma(\gamma+1)}{4} M^2 \frac{dZ}{dx}^2 + \frac{\gamma(\gamma+1)}{12} M^3 \frac{dZ}{dx}^3 \right\} \tag{20}$$

Equating the steady CFD Navier-Stokes coefficient of pressure with Eq.(20) yields a third order polynomial for $\frac{dZ}{dx}$,

$$C_{p,PT}(x) - C_{p,NS}(x) = 0 \tag{21}$$

Solving this equation at each surface grid point results in two complex roots and one real root, which represents the slope of the effective airfoil shape at that grid point. The effective shape can then be obtained by integrating the slope along the length of the airfoil.

RESULTS AND DISCUSSION

The results presented in this section provide a validation of CFL3D for the hypersonic regime, and also contribute to the fundamental understanding of hypersonic aeroelasticity. By comparing results for Euler, Navier-Stokes and piston theory, one can identify the importance of viscosity, and the effectiveness of piston theory in approximating the aeroelastic behavior of a double wedge airfoil in inviscid flow.

The double wedge airfoil is characterized by the following parameters: $t_h/b = 0.025$; $m = 51.833$ kg/m; $\omega_h = 50$ rad/sec; and $\omega_\alpha = 125$ rad/sec. Figure 5 depicts the flutter boundaries of a double wedge airfoil at various altitudes, as a function of the offset a, for the operating envelope of a typical hypersonic vehicle, at zero angle of attack, based on piston theory. The mass ratios for the various altitudes are given in Table 1. Two different configurations of the double wedge airfoil, given in Table 2, were selected for calculations using CFL3D. For flight in the

Mach number range of 5-15, the height selected for the flutter calculations of the two configurations was 70,000 feet. At this altitude, the flutter boundaries are at M=9.21 for configuration A and at M=14.55 for configuration B. Hence, appropriate computational points selected for this study were Mach numbers 7, 10 and 15 at 70,000 feet, with Reynolds numbers of 5.058×10^6, 7.226×10^6 and 1.084×10^7, respectively.

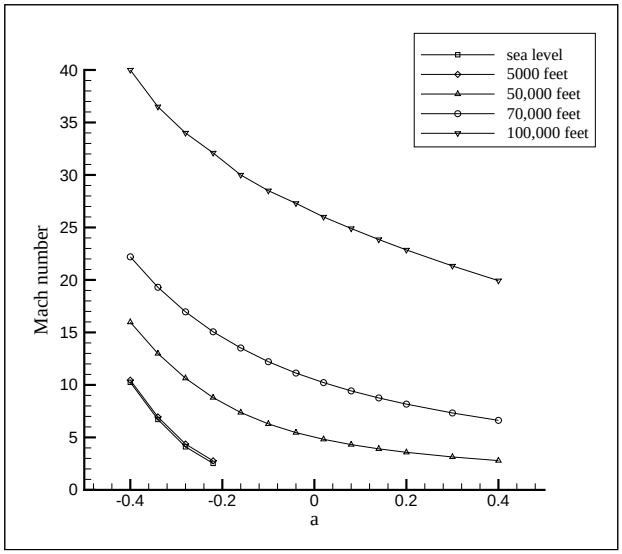

Figure 5. FLUTTER BOUNDARIES OF A DOUBLE WEDGE AIRFOIL AT ZERO ANGLE OF ATTACK, WITH $x_\alpha = 0.2$.

Table 1. MASS RATIOS AT VARIOUS ALTITUDES.

Altitude (ft)	Mass Ratio (μ_m)
0	13.47
5,000	15.63
50,000	88.37
70,000	232.68
100,000	942.60

Selection of Time-step Size

The time-step required for accurate prediction of the aeroelastic response is important in computational aeroelasticity studies. However, selection of an extremely small time-step also requires significant computational resources. Therefore the optimal time-step, determined by a trade-off between accuracy and practical feasibility, was established by a concise numerical study.

Table 2. NONDIMENSIONAL GEOMETRIC AND STRUCTURAL PARAMETERS.

Parameter	Configuration A	Configuration B
$\frac{\omega_h}{\omega_\alpha}$	0.4	0.4
x_α	0.2	0.2
r_α	0.5	0.5
a	0.1	-0.2

In an aeroelastic system with a linear structural operator, the time-step limitation is mainly governed by the unsteady fluid calculations. Therefore, a simulation based on prescribed motion was used to select an appropriate time-step size for each of the flight conditions. To determine the proper step size, the unsteady lift, moment and drag coefficients ($C_L(t)$, $C_{My}(t)$ and $C_D(t)$), due to prescribed motion were computed, and the time-step selected was based on the convergence of these unsteady aerodynamic coefficients. In studying the behavior of these coefficients while varying the step size, it was found that the lift coefficient C_L has the smallest degree of sensitivity to the time-step. For aeroelastic simulations, the lift is the dominant quantity (since drag does not appear in the aeroelastic calculations for the double wedge airfoil). Therefore, it might be expected that the time-step size should be determined primarily based on the behavior of the C_L curves. For the double wedge airfoil geometry, the moment due to lift ($C_L \cdot x_\alpha$) has the same order of magnitude as the moment coefficient, and hence the accuracy of C_{My} is comparable in importance to the accuracy in C_L.

For simulations using Euler aerodynamics, the responses were found to be independent of time-step size when the time-step was smaller than 0.001 sec. To identify the maximum time-step for a viscous aeroelastic simulation, a maximum time-step for a viscous forced-motion simulation was found. This value set an upper limit for the time-step size used in the aeroelastic simulations. Simulations were carried out at 10, 20 and 30 Hz, with a maximum rotation of 1° and 2°, at various altitudes. Results from simulations carried out at 70,000 feet and Mach 10, with maximum rotation of 2° at 20 Hz, are shown in Fig.6. In an aeroelastic simulation, the phase difference between the oscillations in $C_L(t)$ and $C_{My}(t)$ plays a very important role in the stability of the system. A phase difference in the oscillations in $C_L(t)$, $C_{My}(t)$ and $C_D(t)$ in a forced-motion simulation would lead to incorrect aeroelastic behavior at those flight conditions. Hence, when viscosity is considered, C_D is a better indicator of convergence than C_L, even though C_D plays no role in this particular aeroelastic problem. This is because C_D is the best indicator of a phase difference between the various coefficients in a prescribed motion simulation. It was found that the errors in magnitude and phase were not strongly affected by the frequency or magnitude

of the oscillations at a given altitude. The results of this study are summarized in Table 3.

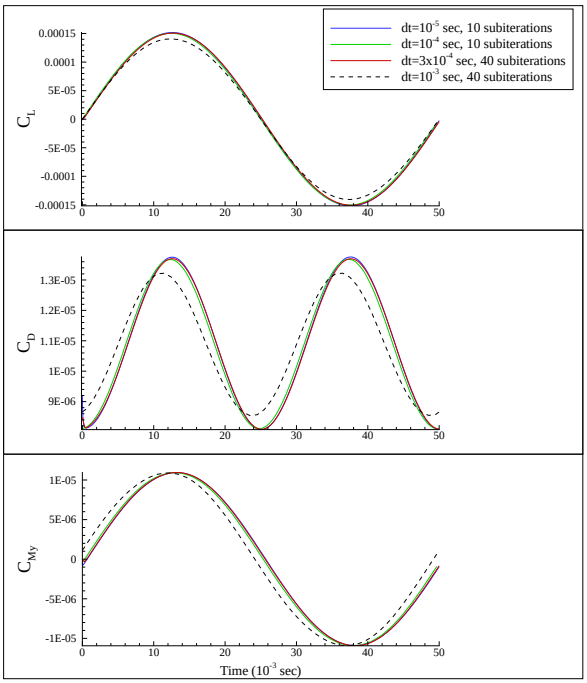

Figure 6. RESULTS FOR FORCED MOTION AT MACH 10 AND 70,000 FEET, WITH $\theta_{max} = 2°$ AT 20 HZ.

Table 3. SUGGESTED TIME-STEP SIZES AND CORRESPONDING NUMBER OF SUBITERATIONS FOR VISCOUS AEROELASTIC SIMULATIONS.

Altitude (ft)	Mach no.	Time-step (sec)	Subiterations
50,000	5.0	0.001	10
70,000	10.0	0.0003	40
100,000	10.0	0.0001	40

Aeroelastic Behavior of the Double Wedge Airfoil

The results for the aeroelastic response of the double wedge airfoil with 2.86° wedge angle using different aerodynamic models, is shown in Figs. 7-10. In some of the figures, time histories end abruptly, due to the inability of the mesh deformation algorithm in CFL3D to track the increasingly large displacements of an unstable system. Figure 7 shows the responses of configuration A at M=7.0. From this figure, it is evident that while piston theory predicts a stable system, both the Euler and Navier-Stokes solutions are unstable. This implies that both Euler and Navier-Stokes aerodynamic models produce aeroelastic results that are more conservative than piston theory for this particular case.

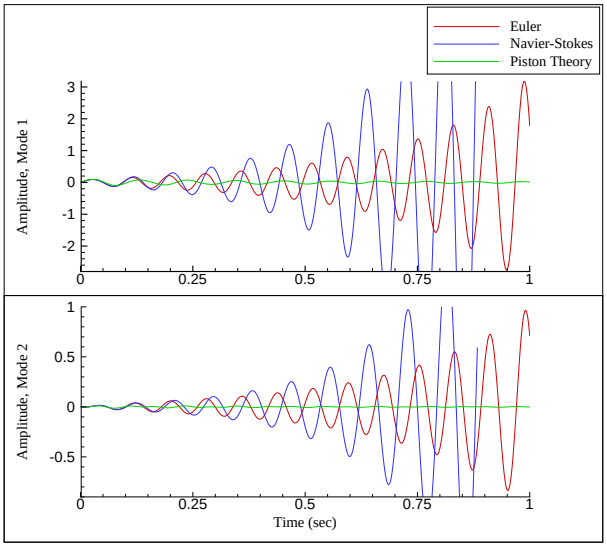

Figure 7. AEROELASTIC RESULTS FOR THE DOUBLE WEDGE AIRFOIL, AT M=7.0 AND AN ALTITUDE OF 70,000 FEET, CONFIGURATION A.

For configuration B, Figs. 8-10 indicate that differences in system responses from the three aerodynamic models are minor at Mach numbers well below the piston theory flutter boundary, but the differences increase with Mach number. At $M = 7.0$, all three aerodynamic models show comparable responses. Furthermore, when the Mach number is increased to $M = 10.0$, the Navier-Stokes response is near critical, while the other two are more stable. However, Euler and piston theory responses are still comparable. When the Mach number is increased to $M = 15.0$, all three aerodynamic models predict unstable responses, with different levels of damping. The increases in differences emphasize the important role of aerodynamic nonlinearities and viscosity with increasing Mach numbers.

These results also illustrate that inspection of the aeroelastic response curves provides only a partial answer. To better understand the differences between aeroelastic results based on piston theory, Euler and Navier-Stokes solutions, actual aeroelastic stability boundaries based on system damping need to be established.

The effect of increasing the wedge angle (or thickness) of the airfoil is depicted in Figs. 11 and 12, at M=10.0 and 70,000 feet. For a wedge angle of 4°, it is shown in Fig. 11 that using Navier-Stokes aerodynamics produces an unstable system, while

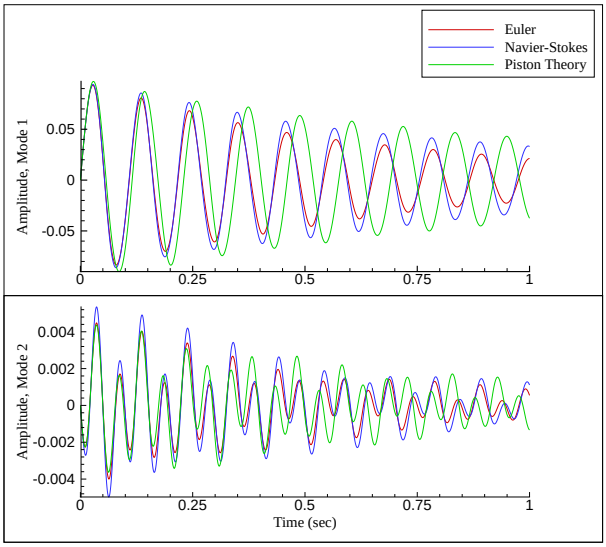

Figure 8. AEROELASTIC RESULTS FOR THE DOUBLE WEDGE AIRFOIL, AT M=7.0 AND AN ALTITUDE OF 70,000 FEET, CONFIGURATION B.

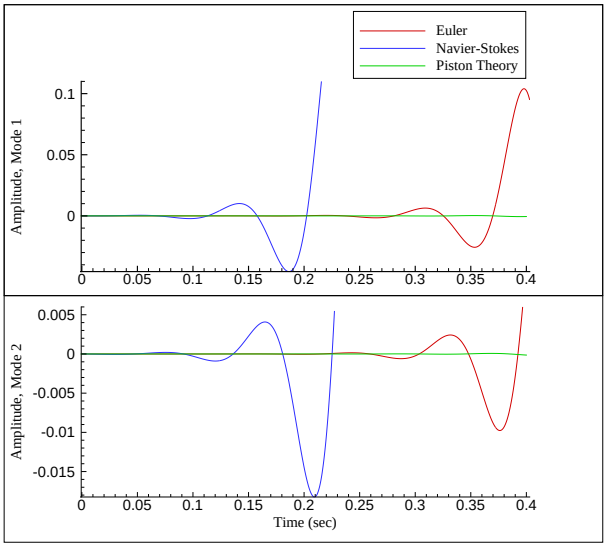

Figure 10. AEROELASTIC RESULTS FOR THE DOUBLE WEDGE AIRFOIL, AT M=15.0 AND AN ALTITUDE OF 70,000 FEET, CONFIGURATION B.

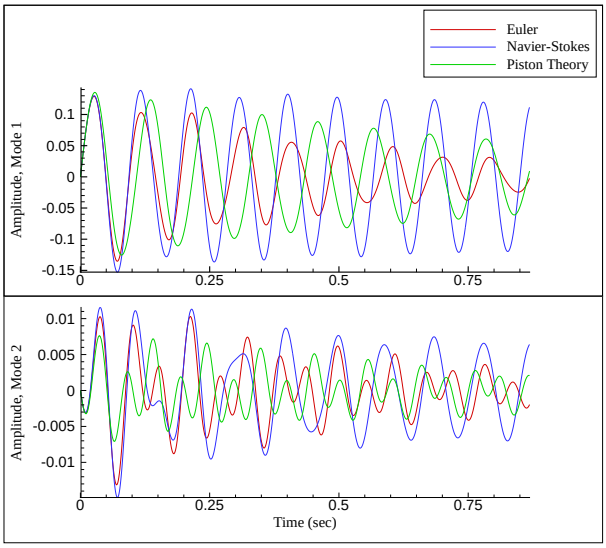

Figure 9. AEROELASTIC RESULTS FOR THE DOUBLE WEDGE AIRFOIL, AT M=10.0 AND AN ALTITUDE OF 70,000 FEET, CONFIGURATION B.

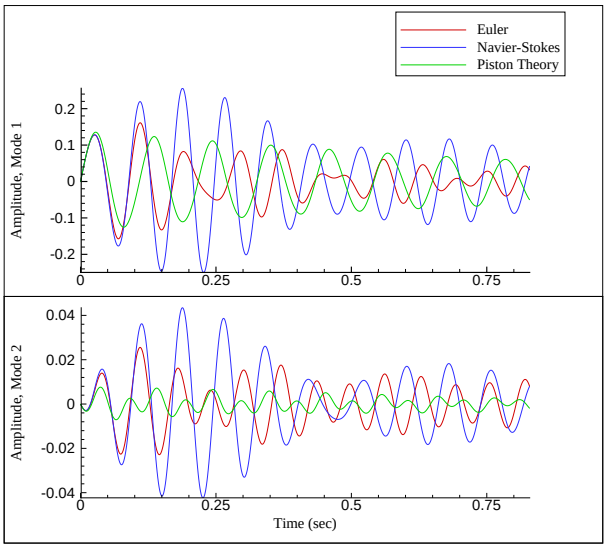

Figure 11. AEROELASTIC RESULTS FOR THE DOUBLE WEDGE AIRFOIL, AT M=10.0 AND AN ALTITUDE OF 70,000 FEET, CONFIGURATION B, WEDGE ANGLE=4°.

the other two aerodynamic models produce a lightly damped response. When the wedge angle is increased to 6°, as shown in Fig. 12, both Euler and Navier-Stokes aerodynamics predict a very unstable system, while the results based on piston theory still show a stable system.

The effective shapes of the double wedge airfoil with 2.86° wedge angle, modified due to the presence of the boundary layer at Mach 5.0, 10.0 and 15.0, are shown in Fig. 13. The effective geometries are calculated from steady CFD Navier-Stokes pressure data, as described previously. Results using the effective airfoil shape are shown in Figs. 14-16, also at M=10.0 and 70,000 feet. Figure 14 compares the results for the double wedge air-

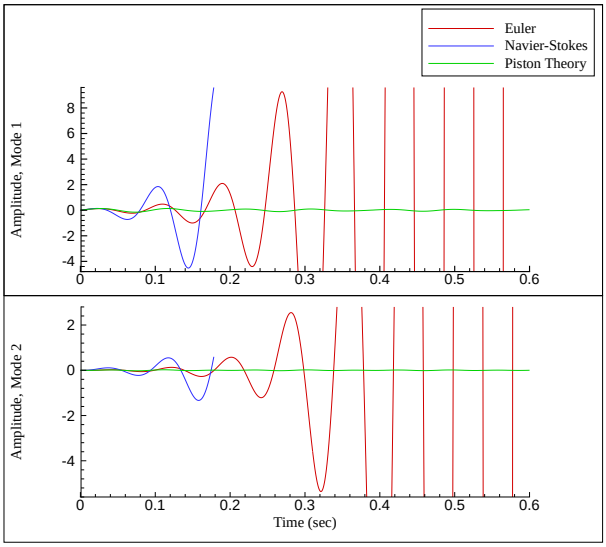

Figure 12. AEROELASTIC RESULTS FOR THE DOUBLE WEDGE AIRFOIL, AT M=10.0 AND AN ALTITUDE OF 70,000 FEET, CONFIGURATION B, WEDGE ANGLE=6°.

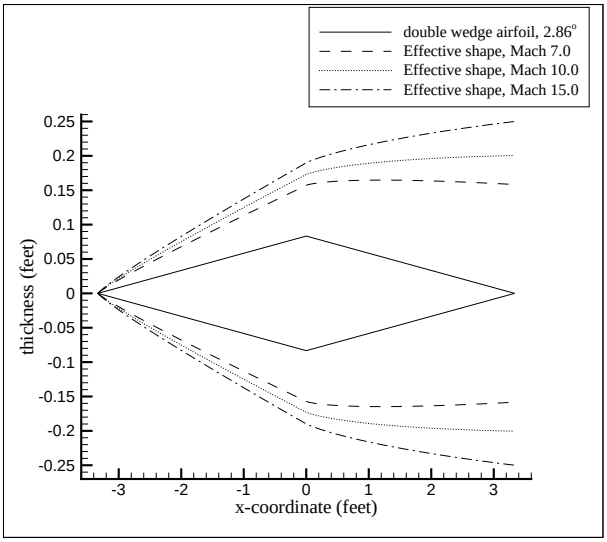

Figure 13. EFFECTIVE SHAPES OF THE DOUBLE WEDGE AIRFOIL WITH 2.86°WEDGE ANGLE.

foil with 2.86° wedge angle (standard geometry), while Fig. 15 compares the results for a 4°wedge angle, and Fig. 16 shows the results for a 6°wedge angle. In all three cases, the Navier-Stokes model predicts larger modal amplitudes than piston theory with the effective shape. Furthermore, at the smallest wedge angle, the piston theory model has a higher level of damping than the Navier-Stokes model. When the wedge angle is increased to 4°, the Navier-Stokes model predicts a response with a beat phenomenon, therefore it is difficult to identify the degree of damping. However, the piston theory model predicts stable system behavior. At the 6°wedge angle, both models predict unstable behavior. It should also be noted that at the 6°wedge angle, piston theory without the effective shape predicted a stable response.

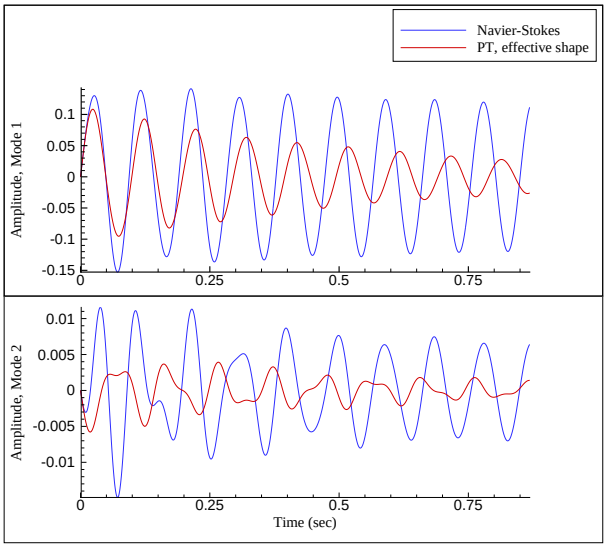

Figure 14. AEROELASTIC RESULTS FOR THE DOUBLE WEDGE AIRFOIL, AT M=10.0 AND AN ALTITUDE OF 70,000 FEET, CONFIGURATION B, WEDGE ANGLE=2.86°. COMPARISON OF NAVIER-STOKES RESULTS WITH EFFECTIVE SHAPE USING PISTON THEORY.

Due to these differences, and limitation of results generated, it is apparent that more study is needed to fully understand the capability of piston theory with an effective shape in accurately capturing viscous effects.

CONCLUSIONS

Based on the limited amount of numerical results presented in this paper, the following conclusions can be stated.

1. The time steps to be used in computational aeroelasticity studies are strongly dependent on the unsteady aerodynamic model used. Using a viscous flow based on the Navier-Stokes equations requires substantially smaller time-step sizes than those used for an Euler solution.
2. Aeroelastic behavior is sensitive to the unsteady aerodynamic model used. For the cases considered, results based on piston theory are more stable than those from Euler and Navier-Stokes based aerodynamic loads.

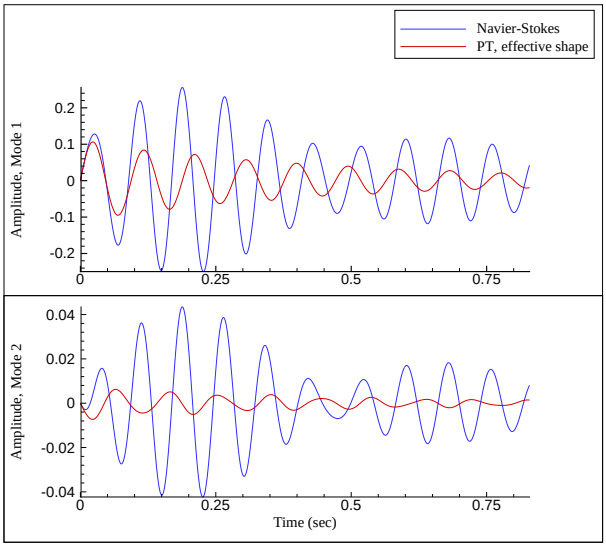

Figure 15. AEROELASTIC RESULTS FOR THE DOUBLE WEDGE AIRFOIL, AT M=10.0 AND AN ALTITUDE OF 70,000 FEET, CONFIGURATION B, WEDGE ANGLE=4°. COMPARISON OF NAVIER-STOKES RESULTS WITH EFFECTIVE SHAPE USING PISTON THEORY.

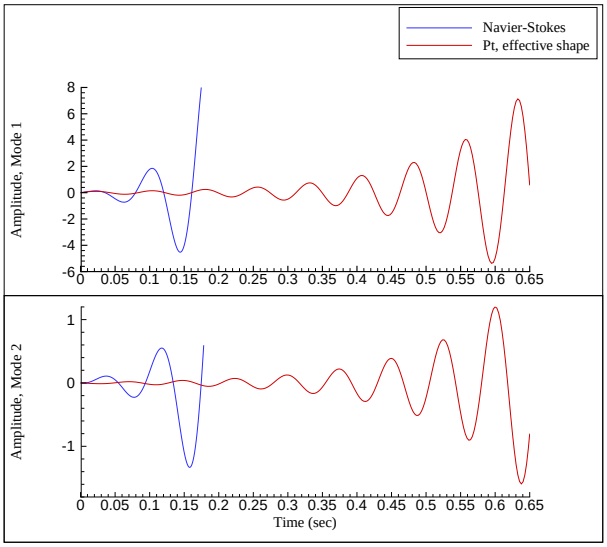

Figure 16. AEROELASTIC RESULTS FOR THE DOUBLE WEDGE AIRFOIL, AT M=10.0 AND AN ALTITUDE OF 70,000 FEET, CONFIGURATION B, WEDGE ANGLE=6°. COMPARISON OF NAVIER-STOKES RESULTS WITH EFFECTIVE SHAPE USING PISTON THEORY.

3. Aeroelastic response results using third order piston theory and exact Euler solutions are fairly close, and predict similar response.
4. Airfoil shapes modified by the presence of a static boundary layer produce an aeroelastic response that differs substantially from that based on the solution of the Navier-Stokes equations.
5. The results presented can be considered to provide a partial validation of the CFL3D code for the hypersonic flow regime.

ACKNOWLEDGEMENT

The authors wish to express their gratitude to NASA Langley Research Center for the CFL3D code and thank Drs. R. Bartels and R. Biedron for their help in using this code. This research is funded by AFOSR under grant number F49620-01-1-0158 with Dr. D. Mook as program manager.

REFERENCES

[1] Xue, D.Y. and Mei, C., "Finite Element Two-Dimensional Panel Flutter at High Supersonic Speeds and Elevated Temperature," AIAA Paper No. 90-0982, *Proc. 31st AIAA/ASME/ASCE/AHS/ASC Structures, Structural Dynamics and Materials Conference*, 1990, pp. 1464–1475.

[2] Gray, E.G. and Mei, C., "Large-Amplitude Finite Element Flutter Analysis of Composite Panels in Hypersonic Flow," AIAA Paper No. 92-2130, *Proc. 33rd AIAA/ASME/ASCE/AHS/ASC Structures, Structural Dynamics and Materials Conference*, Dallas, TX, April 16-17 1992, pp. 492–512.

[3] Abbas, J.F. and Ibrahim,R.A., "Nonlinear Flutter of Orthotropic Composite Panel Under Aerodynamic Heating," *AIAA J.*, Vol. 31, No. 8, No. 8, 1993, pp. 1478–1488.

[4] Bein, T., Friedmann, P., Zhong, X., and Nydick, I., "Hypersonic Flutter of a Curved Shallow Panel with Aerodynamic Heating," AIAA Paper No. 93-1318, *Proc. 34th AIAA/ASME/ASCE/AHS/ASC Structures, Structural Dynamics and Materials Conference*, La Jolla, CA, April 19-22 1993.

[5] Nydick, I., Friedmann, P.P., and Zhong, X., "Hypersonic Panel Flutter Studies on Curved Panels," AIAA Paper no. 95-1485, *Proc. 36th AIAA/ASME/ASCE/AHS/ASC Structures, Structural Dynamics and Materials Conference*, New Orleans, LA, April 1995, pp. 2995–3011.

[6] Mei, C., Abdel-Motagly, K., and Chen, R., "Review of Nonlinear Panel Flutter at Supersonic and Hypersonic Speeds," *Applied Mechanics Reviews*, 1998.

[7] Ricketts, R., Noll, T., Whitlow, W., and Huttsell,L., "An Overview of Aeroelasticity Studies for the National Aerospace Plane," AIAA Paper No. 93-1313, *Proc. 34th AIAA/ASME/ASCE/AHS/ASC Structures, Structural Dynamics and Materials Conference*, La Jolla, CA, April 19-22 1993, pp. 152 – 162.

[8] Scott, R.C. and Pototzky, A.S., "A Method of

Predicting Quasi-Steady Aerodynamics for Flutter Analysis of High Speed Vehicles Using Steady CFD Calculations," AIAA Paper No. 93-1364, *Proc. 34th AIAA/ASME/ASCE/AHS/ASC Structures, Structural Dynamics and Materials Conference*, La Jolla, CA, April 19-22 1993, pp. 595–603.

[9] Spain, C., Zeiler, T.A., Bullock, E., and Hodge, J.S., "A Flutter Investigation of All-Moveable NASP-Like Wings at Hypersonic Speeds," AIAA Paper No. 93-1315, *Proc. 34th AIAA/ASME/ASCE/AHS/ ASC Structures, Structural Dynamics and Materials Conference*, La Jolla, CA, April 19-22 1993.

[10] Spain, C., Zeiler, T.A., Gibbons, M.D., Soistmann, D.L., Pozefsky, P., DeJesus, R.O., and Brannon,C.P., "Aeroelastic Character of a National Aerospace Plane Demonstrator Concept," *Proc. 34th AIAA/ASME/ASCE/AHS/ ASC Structures, Structural Dynamics and Materials Conference*, La Jolla, CA, April 19-22 1993, pp. 163–170.

[11] Heeg, J., Zeiler, T., Pototzky, A., Spain, C., and Engelund, W., "Aerothermoelastic Analysis of a NASP Demonstrator Model," AIAA Paper No. 93-1366, *Proc. 34th AIAA/ASME/ASCE/AHS/ ASC Structures, Structural Dynamics and Materials Conference*, La Jolla, CA, April 19-22 1993, pp. 617–627.

[12] Blades, E., Ruth, M., and Fuhrman, D., "Aeroelastic Analysis of the X-34 Launch Vehicle," AIAA Paper No. 99-1352, *Proc. 40th AIAA/ASME/ASCE/AHS/ ASC Structures, Structural Dynamics and Materials Conference*, St. Louis, MO, 1999, pp. 1321–1331.

[13] Nydick, I. and Friedmann, P.P., "Aeroelastic Analysis of a Generic Hypersonic Vehicle," NASA/CP-1999-209136/PT2, *Proc. CEAS/AIAA/ICASE/NASA Langley International Forum on Aeroelasticity and Structural Dynamics*, Williamsburg, VA, June 22-25 1999, pp. 777–810.

[14] Gupta, K.K., Voelker, L.S., Bach, C., Doyle, T., and Hahn, E., "CFD-Based Aeroelastic Analysis of the X-43 Hypersonic Flight Vehicle," AIAA Paper No. 2001-0712, *39th Aerospace Sciences Meeting & Exhibit*, 2001.

[15] Berry, S.A., Horvath, T.J., Hollis, B.R., Thompson, R.A., and Hamilton, H.H., "X-33 Hypersonic Boundary Layer Transition," AIAA Paper No. 99-3560, *33rd AIAA Thermophysics Conference*, Norfolk, VA, June 28 - July 1 1999.

[16] Riley, C.J., Kleb, W.L., and Alter, S.J., "Aeroheating Predictions for X-34 Using An Inviscid-Boundary Layer Method," AIAA 98-0880, *36th Aerospace Sciences Meeting & Exhibit*, Reno, NV, January 1998.

[17] Thuruthimattam, B.J., Friedmann, P.P., McNamara, J.J., and Powell, K.G., "Aeroelasticity of a Generic Hypersonic Vehicle," AIAA Paper No. 2002-1209, *Proc. 43rd AIAA/ASME/ASCE/AHS Structures, Structural Dynamics and Materials Conference*, Denver, CO, April 2002.

[18] Bousman, W.G. and Winkler, D.J., "Application of the Moving-Block Analysis," AIAA 81-0653, *Proceedings of the AIAA Dynamics Specialist Conference*, Atlanta, GA, April 1981, pp. 755–763.

[19] Krist, S.L., Biedron, R.T., and Rumsey, C.L., "CFL3D User's Manual (Version 5.0)," NASA, TM 1998-208444, 1997.

[20] Robinson, B.A., Batina, J.T., and Yang, H.T., "Aeroelastic Analysis of Wings Using the Euler Equations with a Deforming Mesh," *Journal of Aircraft*, Vol. 28, November 1991, pp. 778–788.

[21] Cunningham, H.J., Batina, J.T., and Bennett, R.M., "Modern Wing Flutter Analysis by Computational Fluid Dynamic Methods," *Journal of Aircraft*, Vol. 25, No. 10, No. 10, 1989, pp. 962–968.

[22] Lee-Rausch, E.M. and Batina, J.T., "Wing Flutter Boundary Prediction Using Unsteady Euler Aerodynamic Method," AIAA Paper No. 93-1422, *Proc. 34th AIAA/ASME/ASCE/AHS Structures, Structural Dynamics and Materials Conference*, 1993, pp. 1019–1029.

[23] Lee-Rausch, E.M. and Batina, J.T., "Calculation of AGARD Wing 445.6 Flutter Using Navier-Stokes Aerodynamics," AIAA Paper No. 93-3476, *Proc. AIAA 11th Applied Aerodynamics Conference*, Hampton, VA, August 9-11 1993.

[24] Ashley, H. and Zartarian, G., "Piston Theory - A New Aerodynamic Tool for the Aeroelastician," *Journal of the Aeronautical Sciences*, Vol. 23, No. 12, No. 12, 1956, pp. 1109–1118.

[25] Lighthill, M.J., "Oscillating Airfoils at High Mach Numbers," *Journal of the Aeronautical Sciences*, Vol. 20, No. 6, June 1953.

[26] Anderson, J.D., *Hypersonic and High Temperature Gas Dynamics*, New York, McGraw-Hill, 1989.